Editors' Suggestion | Featured in Physics

Extending Solid-State Calculations to Ultra-Long-Range Length Scales

T. Müller,[1] S. Sharma,[2] E. K. U. Gross,[3] and J. K. Dewhurst[4,*]
[1]Max-Planck-Institut für Mikrostrukturphysik, Weinberg 2, 06120 Halle, Germany
[2]Max-Born-Institut fr Nichtlineare Optik und Kurzzeitspektroskopie, Max-Born-Strasse 2A, 12489 Berlin, Germany
[3]Fritz Haber Center for Molecular Dynamics, Institute of Chemistry, The Hebrew University of Jerusalem, 91904 Jerusalem, Israel
[4]Max-Planck-Institut für Mikrostrukturphysik, Weinberg 2, 06120 Halle, Germany

(Received 14 September 2020; accepted 2 November 2020; published 16 December 2020)

We present a method that enables solid-state density functional theory calculations to be applied to systems of almost unlimited size. Computations of physical effects up to the micron length scale but which nevertheless depend on the microscopic details of the electronic structure, are made possible. Our approach is based on a generalization of the Bloch state, which involves an additional sum over a finer grid in reciprocal space around each **k** point. We show that this allows for modulations in the density and magnetization of arbitrary length on top of a lattice-periodic solution. Based on this, we derive a set of ultra-long-range Kohn-Sham equations. We demonstrate our method with a sample calculation of bulk LiF subjected to an arbitrary external potential containing nearly 3500 atoms. We also confirm the accuracy of the method by comparing the spin density wave state of bcc Cr against a direct supercell calculation starting from a random magnetization density. Furthermore, the spin spiral state of γ-Fe is correctly reproduced.

DOI: 10.1103/PhysRevLett.125.256402

Density functional theory (DFT) [1] has had a tremendous impact on solid-state physics and is, due to its computational efficiency, at the heart of modern computer based material research. Since its original proposal, further developing DFT has been an ongoing process. Extensions to DFT typically include extra densities in addition to the charge density, such as the magnetization [2], current density [3], or the superconducting order parameter [4]. Another fundamental extension of DFT was the generalization to time-dependent systems [5] enabling accurate calculations of excited-state properties and strongly driven systems. While these extensions allowed for a more in-depth understanding of microscopic properties, not much progress has been made in applying DFT to effects in solids occurring on larger, mesoscopic length scales. Such effects include long-ranged quasiparticles, magnetic domains, or spatially dependent electric fields. As DFT is a formally exact theory, the underlying physics for such phenomena is readily at hand, yet actual calculations remain very difficult. In a typical calculation a single unit cell is solved with periodic boundary conditions, and thus effects extending far beyond the size of a single unit cell are lost. While it is, in principle, possible to use ever larger supercells, in practice one quickly reaches the limit of computational viability. This is mostly due to the poor scaling with the number of atoms, $\sim\mathcal{O}(N_{\mathrm{atom}}^3)$, which plagues all computer programs with a systematic basis set and limits calculations to systems containing a maximum of $\sim$1000 atoms. Recent progress based on linear scaling approaches [6] was able to increase the computable system size considerably. Linear scaling approaches, however, require a "nearsightedness" of the system. While this might be fulfilled for effects strictly related to the charge density, this is certainly not fulfilled for large magnetic systems, such as magnetic domains.

In this Letter we propose a fundamentally different approach to drastically extend the length scale of DFT calculations without significantly increasing the computational cost. Our approach relies on altered Bloch states and can be understood as a generalization of the spin-spiral ansatz [7], which emerges as a special case of our ansatz. In the spin-spiral ansatz, a momentum-dependent phase is added to the normal Bloch state. It then becomes possible to compute a large, extended spiraling magnetic moment with a single unit cell. While this is computationally very efficient, it is, at the same time, the biggest limitation of the spin-spiral ansatz: It allows only for a change in the direction of the magnetization while the magnitude of the magnetization and the charge density remain unaltered. We overcome this limitation by introducing an additional sum in the Bloch states over a finer grid in reciprocal space around each **k** point. The resulting densities then become a Fourier series with a controllable periodicity, which may extend far beyond the length scale of a single unit cell.

The systems we will focus on in this Letter are described by the Kohn-Sham (KS) Hamiltonian of spin-density functional theory (atomic units are used throughout):

$$\hat{H}_0 = -\frac{\nabla^2}{2} + v_s(\mathbf{r}) + \mathbf{B}_s(\mathbf{r}) \cdot \boldsymbol{\sigma}. \tag{1}$$

The KS potential $v_s(\mathbf{r}) = v_{\text{ext}}(\mathbf{r}) + v_H(\mathbf{r}) + v_{\text{xc}}(\mathbf{r})$ consists of an external potential v_{ext}, a Hartree potential [8] v_H and an exchange-correlation (xc) potential v_{xc}. Similarly, the KS magnetic field $\mathbf{B}_s(\mathbf{r}) = (1/2c)\mathbf{B}_{\text{ext}}(\mathbf{r}) + \mathbf{B}_{\text{xc}}(\mathbf{r})$ can be decomposed into an external field $\mathbf{B}_{\text{ext}}$ and an xc field $\mathbf{B}_{\text{xc}}$. We will start off by extending the KS wave functions. From that we will derive altered charge and magnetization densities. Finally, we will derive a long-range Hamiltonian and the matrix elements associated with it.

Bloch states of the form $\varphi_{n\mathbf{k}}(\mathbf{r}) = u_{n\mathbf{k}}(\mathbf{r})e^{i\mathbf{k}\cdot\mathbf{r}}$, where $u_{n\mathbf{k}}$ is a lattice-periodic spinor function, are used in standard solid-state calculations. The central idea of our approach is a generalization of this Bloch state to include long-range modulations. Our ultra-long-range ansatz employs, in addition to a momentum-dependent phase [7], momentum-dependent expansion coefficients which allow for changes in magnitude and direction of the spin and charge densities from cell to cell. For a fixed $\mathbf{k}$ vector our new Bloch-like state reads

$$\Phi^{\mathbf{k}}_{\alpha}(\mathbf{r}) = \frac{1}{\sqrt{N_u}} \sum_{n\boldsymbol{\kappa}} c^{\alpha}_{n\mathbf{k}+\boldsymbol{\kappa}} \begin{pmatrix} u^{\uparrow}_{n\mathbf{k}}(\mathbf{r}) \\ u^{\downarrow}_{n\mathbf{k}}(\mathbf{r}) \end{pmatrix} e^{i(\mathbf{k}+\boldsymbol{\kappa})\cdot\mathbf{r}}, \tag{2}$$

where $u^{\uparrow\downarrow}_{n\mathbf{k}}$ are the normalized orbitals of a lattice-periodic system, n is a band index, and $\mathbf{k}$ a reciprocal space vector, $c^{\alpha}_{n\mathbf{k}+\boldsymbol{\kappa}}$ are complex coefficients to be determined variationally and α labels a particular long-range state. The vectors $\boldsymbol{\kappa}$ live on a finer grid around each $\mathbf{k}$ point in reciprocal space [Fig. 1(a)], which we use to sample long-range effects. Finally, N_u is a normalization factor that is equal to the number of unit cells on which $\Phi^{\mathbf{k}}_{\alpha}$ is periodic. Note that we have used the lattice periodic parts of the orbitals at $\mathbf{k}$ and not $\mathbf{k}+\boldsymbol{\kappa}$. In principle, both are complete basis sets capable of expanding any lattice-periodic function. In practice, the choice of using $u^{\uparrow\downarrow}_{n\mathbf{k}}$ over $u^{\uparrow\downarrow}_{n\mathbf{k}+\boldsymbol{\kappa}}$ is more efficient for determining the density, magnetization, and Hamiltonian matrix elements.

From this wave function, we can construct a charge and magnetization density

$$\rho(\mathbf{r}) = \frac{1}{N_k} \sum_{\mathbf{k},\alpha} f^{\mathbf{k}}_{\alpha} \Phi^{\mathbf{k}\dagger}_{\alpha}(\mathbf{r}) \Phi^{\mathbf{k}}_{\alpha}(\mathbf{r}), \tag{3}$$

$$\mathbf{m}(\mathbf{r}) = \frac{1}{N_k} \sum_{\mathbf{k},\alpha} f^{\mathbf{k}}_{\alpha} \Phi^{\mathbf{k}\dagger}_{\alpha}(\mathbf{r}) \boldsymbol{\sigma} \Phi^{\mathbf{k}}_{\alpha}(\mathbf{r}), \tag{4}$$

with the number of $\mathbf{k}$ points $N_{\mathbf{k}}$ and the ultra-long-range occupation numbers $f^{\mathbf{k}}_{\alpha}$ associated with the orbitals $\Phi^{\mathbf{k}}_{\alpha}$. The charge and magnetization density obtained from this wave function take the form $\rho(\mathbf{r}) = \sum_{\mathbf{Q}} \rho_{\mathbf{Q}}(\mathbf{r}) e^{i\mathbf{Q}\cdot\mathbf{r}}$ and $\mathbf{m}(\mathbf{r}) = \sum_{\mathbf{Q}} \mathbf{m}_{\mathbf{Q}}(\mathbf{r}) e^{i\mathbf{Q}\cdot\mathbf{r}}$, with $\mathbf{Q} = \boldsymbol{\kappa} - \boldsymbol{\kappa}'$. These partial densities $\rho_{\mathbf{Q}}$ and $\mathbf{m}_{\mathbf{Q}}$ are complex in general and act as lattice-periodic Fourier coefficients. The resulting real-space densities $\rho(\mathbf{r})$ and $\mathbf{m}(\mathbf{r})$ are real functions, which,

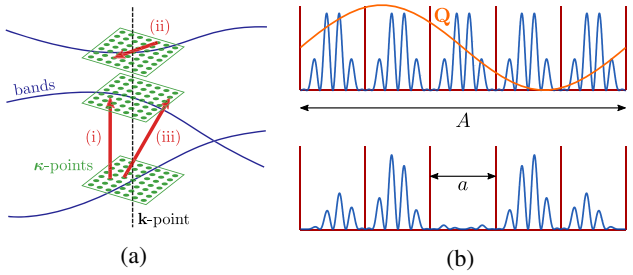

FIG. 1. (a) Schematic of the $\boldsymbol{\kappa}$-point grid. For each $\mathbf{k}$ point (black dashed line) all bands (blue) are augmented with a fine grid of $\boldsymbol{\kappa}$ points (green). Three different types of couplings between $\boldsymbol{\kappa}$ points corresponding to different length scales are possible. (i) A coupling between two identical $\boldsymbol{\kappa}$ points but with different band indices (ii) a coupling between different $\boldsymbol{\kappa}$ points sharing the same band index, and (iii) a coupling between different $\boldsymbol{\kappa}$ points with different band indices. The maximum length scale of the calculation may be chosen by adjusting the $\boldsymbol{\kappa}$-point grid. (b) A schematic of the long-range approach. The red lines indicate unit cells. The lattice periodic density $\rho_{\mathbf{Q}}$ (blue) is altered by a $\mathbf{Q}$-dependent modulation (orange) with a different periodicity. The result (lower graph) depends on both, the long-range modulation and the lattice periodic solution. a is the lattice constant of a unit cell and A is the lattice constant of the ultracell, which is the smallest cell that contains the full long-range solution.

depending on the values of $\mathbf{Q}$, will have a periodicity larger than the length scale of a unit cell [Fig. 1(b)]. By adjusting the underlying $\boldsymbol{\kappa}$ lattice, it is therefore possible to change the $\mathbf{Q}$ vectors and hence allow for variations of arbitrary length in the system. The $\mathbf{Q} = 0$ term deserves special mention, as it corresponds to the full lattice-periodic solution. We emphasize that there is no restriction on the magnitude of $\rho_{\mathbf{Q}}, \mathbf{m}_{\mathbf{Q}}$ and we are thus able to expand arbitrary modulations in the charge and magnetization densities. This is a key difference compared to the spin-spiral ansatz [7] or any down-folding technique.

The Fourier coefficients $\rho_{\mathbf{Q}}$ and $\mathbf{m}_{\mathbf{Q}}$ can be calculated efficiently by first calculating the wave function in Eq. (2) for a subset of unit cells given by a set of real-space lattice vectors $\{\mathbf{R}_i\}$. We choose the $\mathbf{R}_i$ vectors to be the conjugate real-space vectors of the $\mathbf{Q}$ vectors. The wave function in a single unit cell is then given by a sum over n and a fast Fourier transform in $\boldsymbol{\kappa}$ of the coefficients $c^{\alpha}_{n\mathbf{k}+\boldsymbol{\kappa}}$:

$$\Phi^{\mathbf{k}}_{\alpha}(\mathbf{r}+\mathbf{R}_i) \approx e^{i\mathbf{k}\cdot(\mathbf{r}+\mathbf{R}_i)} \sum_{n} \begin{pmatrix} u^{\uparrow}_{n\mathbf{k}}(\mathbf{r}) \\ u^{\downarrow}_{n\mathbf{k}}(\mathbf{r}) \end{pmatrix} \sum_{\boldsymbol{\kappa}} c^{\alpha}_{n\mathbf{k}+\boldsymbol{\kappa}} e^{i\boldsymbol{\kappa}\cdot\mathbf{R}_i}, \tag{5}$$

where $\mathbf{r}$ is restricted to a single unit cell and we have assumed that $|\boldsymbol{\kappa}\cdot\mathbf{r}| \ll 1$. Note also that the normalization constant $1/\sqrt{N_u}$ has been removed. This ensures that observables such as charge and energy are calculated per unit cell rather than per ultracell. From this, we compute the charge and magnetization densities on the same grid, i.e.,

$\rho_i = \rho(\mathbf{r}+\mathbf{R}_i)$ and $\mathbf{m}_i = \mathbf{m}(\mathbf{r}+\mathbf{R}_i)$. This set can then be partially (fast) Fourier transformed to reciprocal space to obtain $\rho_{\mathbf{Q}}(\mathbf{r})$ and $\mathbf{m}_{\mathbf{Q}}(\mathbf{r})$:

$$\rho_{\mathbf{Q}}(\mathbf{r}) = \frac{1}{N_{\mathbf{R}}}\sum_i \rho(\mathbf{r}+\mathbf{R}_i)e^{-i\mathbf{Q}\cdot\mathbf{R}_i},$$
$$\mathbf{m}_{\mathbf{Q}}(\mathbf{r}) = \frac{1}{N_{\mathbf{R}}}\sum_i \mathbf{m}(\mathbf{r}+\mathbf{R}_i)e^{-i\mathbf{Q}\cdot\mathbf{R}_i}. \quad (6)$$

Here $N_{\mathbf{R}}$ denotes the number of $\mathbf{R}$ vectors chosen. With the densities at hand, we will now focus on generalizing the Hamiltonian such that meaningful, nontrivial values for the expansion coefficients $c^{\alpha}_{n\mathbf{k}+\boldsymbol{\kappa}}$ in Eq. (2) are obtained. The ultra-long-range Hamiltonian retains the full lattice periodic KS Hamiltonian $\hat{H}_0$ given in Eq. (1), but also has an additional "modulation" term

$$\hat{H} = \hat{H}_0 + \sum_{\mathbf{Q}} \hat{H}_{\mathbf{Q}}(\mathbf{r})e^{i\mathbf{Q}\cdot\mathbf{r}}. \quad (7)$$

The total Hamiltonian $\hat{H}$ is thus decomposed in the same way as the charge and magnetization densities For a KS system like Eq. (1), our modulation Hamiltonian reads

$$\hat{H}_{\mathbf{Q}}(\mathbf{r}) = V_{\mathbf{Q}}(\mathbf{r}) + \mathbf{B}_{\mathbf{Q}}(\mathbf{r})\cdot\boldsymbol{\sigma}, \quad (8)$$

where $V_{\mathbf{Q}}(\mathbf{r})$ and $\mathbf{B}_{\mathbf{Q}}(\mathbf{r})$ are again complex, lattice periodic Fourier coefficients and contribute to long-ranged versions of the scalar potential and the magnetic field, respectively. In the following we will discuss these coefficients and how to compute them in more detail. We will start with the scalar potential, which can be decomposed into an external potential $V^{\mathrm{ext}}_{\mathbf{Q}}(\mathbf{r})$, a Hartree potential $V^{H}_{\mathbf{Q}}(\mathbf{r})$, and an xc potential $V^{\mathrm{xc}}_{\mathbf{Q}}(\mathbf{r})$. $V^{\mathrm{ext}}_{\mathbf{Q}}(\mathbf{r})$ of an external, long-ranged potential can be freely chosen. The coefficients for the long-ranged Hartree potential $V^{H}_{\mathbf{Q}}(\mathbf{r})$ are obtained from the long-range density

$$V^{H}_{\mathbf{Q}}(\mathbf{r}) = \int d^3r' \frac{\rho_{\mathbf{Q}}(\mathbf{r}')}{|\mathbf{r}-\mathbf{r}'|}e^{-i\mathbf{Q}\cdot(\mathbf{r}-\mathbf{r}')}. \quad (9)$$

This integral may be performed efficiently by further Fourier transforming $\rho_{\mathbf{Q}}(\mathbf{r})$ to $\rho_{\mathbf{Q}}(\mathbf{G})$, where $\mathbf{G}$ is a reciprocal lattice vector. The Hartree potential is then determined directly via $V^{H}_{\mathbf{Q}}(\mathbf{G}) = 4\pi\rho_{\mathbf{Q}}(\mathbf{G})/|\mathbf{G}+\mathbf{Q}|^2$ and can be subsequently Fourier transformed back to real space. This is easily extended to the case of the augmented plane wave basis by using the method of Weinert [8].

Next we will determine the coefficients associated with the xc term. An important difference compared to the Hartree potential is that the xc potential is inherently a nonlinear functional of the densities, therefore the naive approach $V^{\mathrm{xc}}_{\mathbf{Q}} = V_{\mathrm{xc}}[\rho_{\mathbf{Q}}]$ may introduce a mixing of the real and imaginary part of $\rho_{\mathbf{Q}}$. Instead, we first Fourier transform the density to real space, $\rho_{\mathbf{R}_i}(\mathbf{r})$, and then evaluate the xc potential separately for each $\mathbf{R}$ vector. The inverse Fourier transform is then applied to obtain

$$V^{\mathrm{xc}}_{\mathbf{Q}}(\mathbf{r}) = \frac{1}{N_{\mathbf{R}}}\sum_j V_{\mathrm{xc}}[\rho_{\mathbf{R}_j}](\mathbf{r})e^{-i\mathbf{Q}\cdot\mathbf{R}_j}. \quad (10)$$

We note that if the number of $\mathbf{Q}$ or $\mathbf{R}$ vectors is less than the number of unit cells a small error due to the effective interpolation between unit cells is incurred.

The coefficients of the magnetic field $\mathbf{B}_{\mathbf{Q}}$ in Eq. (8) consists of an external field, an xc field, and a dipole-dipole field: $\mathbf{B}_{\mathbf{Q}}(\mathbf{r}) = (1/2c)\mathbf{B}^{\mathrm{ext}}_{\mathbf{Q}}(\mathbf{r}) + \mathbf{B}^{\mathrm{xc}}_{\mathbf{Q}}(\mathbf{r}) + (1/2c)\mathbf{B}^{\mathrm{D}}_{\mathbf{Q}}(\mathbf{r})$. Again, the external magnetic field may be chosen arbitrarily and the xc field can be computed analogously to the xc potential

$$\mathbf{B}^{\mathrm{xc}}_{\mathbf{Q}}(\mathbf{r}) = \frac{1}{N_{\mathbf{R}}}\sum_i \mathbf{B}_{\mathrm{xc}}[\rho_{\mathbf{R}_i},\mathbf{m}_{\mathbf{R}_i}](\mathbf{r})e^{-i\mathbf{Q}\cdot\mathbf{R}_i}. \quad (11)$$

The last term of $\mathbf{B}_{\mathbf{Q}}(\mathbf{r})$ corresponds to the magnetic field associated with the magnetostatic dipole-dipole interaction

$$\mathbf{B}^{\mathrm{D}}_{\mathbf{Q}}(\mathbf{r}) = \frac{1}{2c}\int d^3r' \frac{3\mathbf{e}_{\mathbf{r}-\mathbf{r}'}(\mathbf{m}_{\mathbf{Q}}(\mathbf{r}')\cdot\mathbf{e}_{\mathbf{r}-\mathbf{r}'}) - \mathbf{m}_{\mathbf{Q}}(\mathbf{r}')}{|\mathbf{r}-\mathbf{r}'|^3}e^{-i\mathbf{Q}\cdot(\mathbf{r}-\mathbf{r}')}, \quad (12)$$

where $\mathbf{e}_{\mathbf{r}-\mathbf{r}'}$ is the unit vector along the direction $\mathbf{r}-\mathbf{r}'$. The contribution of the dipole-dipole interaction is typically neglected in DFT calculations as it is usually small in comparison with $\mathbf{B}^{\mathrm{xc}}$, which originates from the Coulomb exchange interaction. However, as the Coulomb exchange interaction is inherently short ranged, the magnetic dipole-dipole interaction is expected to have a significant contribution at larger length scales. We therefore include this term in the modulation Hamiltonian. The derivation of a truly nonlocal, $\mathbf{Q}$-dependent xc potential is beyond the scope of this Letter but has been addressed by Pellegrini *et al.* [9] for the dipole interaction.

We have implemented the ultra-long-range approach in the Elk electronic structure code [10], which is an all electron code using full-potential linearized augmented plane wave (FPLAPW) method. Details of the numerical implementation, such as parameters for the $\mathbf{k}$ point and $\mathbf{Q}$-point grids chosen for the calculations, are given in the Supplemental Material [11]. The scaling of the method is linear in the number of $\mathbf{k}$ points and cubic in κ points. To test our method, we performed two calculations for which the ultracell is small enough to be amenable to supercell calculations so that a detailed comparison is possible. Finally, we demonstrate the efficiency of our method with a calculation which would be considered too large to be treated as a supercell.

(a) Spin spirals in γ-Fe.—The first numerical test deals with the so-called γ phase of Fe. Previous calculations [12]

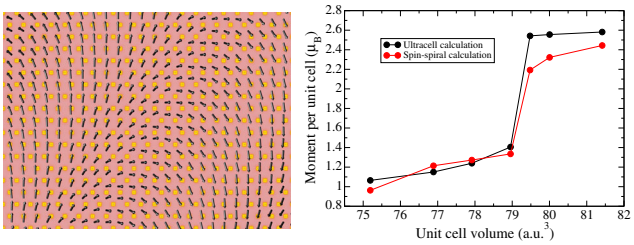

FIG. 2. (a) Ultra-long-range magnetization density of γ-Fe plotted in the plane perpendicular to [001]. The color indicates the magnitude of the magnetization and the arrows indicate the direction. The modulation encompasses 32 unit cells in the [100] direction. (b) Plot of moment against unit cell volume for both the long-range and spin-spiral ansatz.

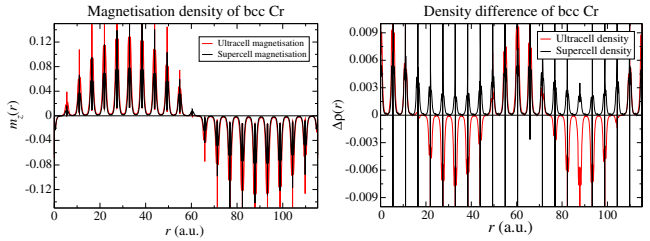

FIG. 3. (a) Magnetization density for bcc Cr over 21 unit cells. (b) Change in density over the same range. For the ultracell, this was generated by setting $\rho_{\mathbf{Q}=0}(\mathbf{r})$ in Eq. (6) to zero. For the supercell, the lattice-periodic density was subtracted leaving just the modulated density.

have shown that the spin-spiral state has the lowest energy compared to several commensurate ferromagnetic and antiferromagnetic structures. The ultra-long-range method allows us to address the question whether the much larger variational freedom associated with the ultracell still yields the spin spiral as ground state. We perform both the traditional spin spiral as well as the ultracell calculations for γ-Fe. Spin-orbit coupling cannot be used consistently with the spin-spiral ansatz but there is no such restriction with the long-range method. However, for the sake of comparison, spin-orbit coupling was not included in the ultracell calculations.

An initial magnetic field is required to break the spin symmetry. To ensure an unbiased calculation, we applied a random field to the ultracell calculation and subsequently reduced it to zero. Nevertheless, the magnetization converged to an ordered state where the magnitude was constant over the ultracell and only the direction varied [Fig. 2(a)]. This corresponds precisely to the lattice parameter and undergoes a transition from $\sim 1\mu_B$ to $\sim 2.5\mu_B$ for this relatively small $\mathbf{Q}$ vector. As may be seen in Fig. 2(b), this behavior is observed for both the ultracell and spin-spiral calculations.

(b) Spin density wave in bcc Cr.—In a second test, we aim at calculating the coupled charge and spin density wave (SDW) state in Cr. The existence of a SDW in Cr is well known and first research dates back to around 1960 [13–15]. Despite this, computing the SDW state within DFT remains difficult and has been the topic of many studies [16–28], with partially conflicting results [29]. It is likely that a SDW is not the true ground state of Cr within DFT [30], however, we will not focus here on the inherent complexities of the system. This state is not achievable by the spin-spiral ansatz because the magnitude of the moment changes but not its direction, thus a supercell calculation is required. Cr is an excellent test scenario, as the periodicity of the SDW is ~20.83 unit cells, which is still well within computational reach of the supercell approach.

For our comparison, we use the LSDA and a lattice parameter of 2.905 Å as suggested by Cottenier *et al.* [29]. Spin-orbit coupling was included for both supercell and ultracell calculations. Our results are shown in Fig. 3. Specifically, Fig. 3(a) shows the comparison of the magnetization in the SDW state, as obtained from the supercell and ultracell calculations. In Fig. 3(b) we present the charge density wave (CDW) which is known to stabilize alongside the SDW with twice the period. While obtaining the CDW in the ultracell is straightforward [as all $\rho_{\mathbf{Q}}(\mathbf{r})$ are known], it is numerically more challenging to extract it for the supercell. We did this by subtracting the density from the calculation of a single unit cell. We obtain the same periodicity in both calculations as well as a comparable magnitude.

(c) Long-range electrostatic potential in LiF.—The previous two examples involved modulations in long-range magnetic order, now we test the method with long-range, external electrostatic fields. This is in anticipation of a future development where ultra-long-range TDDFT calculations are performed in conjunction with Maxwell's equations. To demonstrate the power of our new method, we perform a calculation which is too large for a supercell. Rather than attempting to model a physical phenomenon at this stage, we simply apply an arbitrarily chosen electrostatic potential to an insulator, in this case LiF.

The resultant change in density away from unit cell periodicity is plotted in Fig. 4. As the potential is artificial, the important metric here is the computational effort expended in reaching the self-consistent solution. The rate

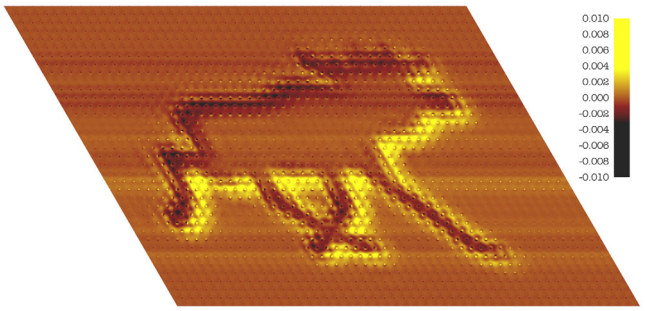

FIG. 4. Self-consistent density without the $\rho_{\mathbf{Q}=0}(\mathbf{r})$ term for a 3456 atom ultracell of LiF with an artificial external potential. The plotting plane is perpendicular to [001] and contains 48×36 unit cells.

of convergence is fairly slow because of the effect of the long-range Coulomb interaction, and thus we performed 170 iterations of the self-consistent loop. The calculation was performed on 480 CPU cores and each iteration took about 40 min. This level of performance for an all-electron calculation indicates that physical phenomena involving modulations of the electronic state over hundreds or thousands of unit cells are within reach of this approach. To estimate the accuracy of the method another example of a given external potential, a sawtooth potential applied to Si, with periodicity small enough to allow comparison with a supercell calculation is given in the Supplemental Material [11]. In both these examples, nuclear degrees of freedom are neglected. However, it would be straightforward to include the effect of atomic displacements in the ultracell via the gradient of the nuclear Coulomb potential.

To summarize, we have developed a method which makes possible the *ab initio* treatment of hitherto uncomputable length scales in solids. This consists of a modified Bloch ansatz and a set of Kohn-Sham equations which have to be solved self-consistently. The underlying lattice of nuclear charges is still periodic on the unit cell length scale but the electronic state can accommodate arbitrary modulations on any length scale. Based on our experience with the all-electron Elk code, we are confident that this method can be efficiently implemented in most existing solid-state electronic structure codes. We demonstrated the capabilities of the novel method by solving an arbitrary external potential applied to nearly 3500 atoms of LiF. Additionally, we showed that our method can reproduce the results obtained by supercell calculations on smaller length scales for two examples of magnetic solids. We do expect the method to become inefficient in cases where both the ultracell is large and a high resolution of density modulations is required, for example, magnetic domains where the length scale of the domain walls is much smaller than the size of the domains themselves. The method presented in this Letter opens up exciting possibilities of future research: it paves the way to calculations of mesoscopic systems, such as magnetic domain walls or skyrmions, which have so far been out of reach for *ab initio* methods like DFT. Furthermore, the novel technique is straightforwardly incorporated in real-time TDDFT calculations which, when combined with the solution of Maxwell's equations, will give access to the propagation of electromagnetic radiation through extended solids and to the dynamics of mesoscopic structures such as plasmonic microantennas within a genuine *ab initio* description.

S. S. and T. M. would like to thank German Research Foundation (DFG) through priority program SPP 1840. E. K. U. G. acknowledges financial support from the European Research Council Advanced Grant FACT (ERC-2017-AdG-788890).

*dewhurst@mpi-halle.mpg.de

[1] P. Hohenberg and W. Kohn, Phys. Rev. **136**, B864 (1964).
[2] U. von Barth and L. Hedin, J. Phys. C **5**, 1629 (1972).
[3] G. Vignale and M. Rasolt, Phys. Rev. Lett. **59**, 2360 (1987).
[4] L. N. Oliveira, E. K. U. Gross, and W. Kohn, Phys. Rev. Lett. **60**, 2430 (1988).
[5] E. Runge and E. K. U. Gross, Phys. Rev. Lett. **52**, 997 (1984).
[6] S. Goedecker, Rev. Mod. Phys. **71**, 1085 (1999).
[7] L. M. Sandratskii, Phys. Status Solidi (b) **136**, 167 (1986).
[8] M. Weinert, J. Math. Phys. (N.Y.) **22**, 2433 (1981).
[9] C. Pellegrini, T. Müller, J. K. Dewhurst, S. Sharma, A. Sanna, and E. K. U. Gross, Phys. Rev. B **101**, 144401 (2020).
[10] The Elk Code, http://elk.sourceforge.net/.
[11] See Supplemental Material at http://link.aps.org/supplemental/10.1103/PhysRevLett.125.256402 for practical implementation of this method in any electronic structure code, the required details like matrix elements.
[12] E. Sjöstedt and L. Nordström, Phys. Rev. B **66**, 014447 (2002).
[13] L. M. Corliss, J. M. Hastings, and R. J. Weiss, Phys. Rev. Lett. **3**, 211 (1959).
[14] V. N. Bykov, V. S. Golovkin, N. V. Ageev, V. A. Levdik, and S. I. Vinogradov, Sov. Phys. Dokl. **4**, 1070 (1960).
[15] A. W. Overhauser, Phys. Rev. **128**, 1437 (1962).
[16] V. Moruzzi, J. Janak, and A. Williams, *Calculated Electronic Properties of Metals*, edited by V. Moruzzi, J. Janak, and A. Williams (Pergamon Press, New York, 1978), pp. 30–159.
[17] J. Kübler, J. Magn. Magn. Mater. **20**, 277 (1980).
[18] H. L Skriver, J. Phys. F **11**, 97 (1981).
[19] N. I. Kulikov and E. Kulatov, J. Phys. F **12**, 2291 (1082).
[20] N. I. Kulikov, M. Alouani, M. A. Khan, and M. V. Magnitskaya, Phys. Rev. B **36**, 929 (1987).
[21] J. Chen, D. Singh, and H. Krakauer, Phys. Rev. B **38**, 12834 (1988).
[22] V. L. Moruzzi and P. M. Marcus, Phys. Rev. B **46**, 3171 (1992).
[23] D. J. Singh and J. Ashkenazi, Phys. Rev. B **46**, 11570 (1992).
[24] K. Hirai, J. Phys. Soc. Jpn. **66**, 560 (1997).
[25] G. Y. Guo and H. H. Wang, Phys. Rev. B **62**, 5136 (2000).
[26] G. Bihlmayer, T. Asada, and S. Blügel, Phys. Rev. B **62**, R11937 (2000).
[27] J. Schfer, E. Rotenberg, S. Kevan, and P. Blaha, Surf. Sci. **454–456**, 885 (2000).
[28] R. Hafner, D. Spisk, R. Lorenz, and J. Hafner, J. Phys. Condens. Matter **13**, L239 (2001).
[29] S. Cottenier, B. De Vries, J. Meersschaut, and M. Rots, J. Phys. Condens. Matter **14**, 3275 (2002).
[30] R. Hafner, D. Spišák, R. Lorenz, and J. Hafner, Phys. Rev. B **65**, 184432 (2002).